


Spin wave dynamics in elliptical dots

R. Dutra, D. E. Gonzalez-Chavez, T. L. Marcondes, and R. L. Sommer
Centro Brasileiro de Pesquisas Físicas, 22290-180 Rio de Janeiro, RJ, Brazil

S. O. Parreiras and M. D. Martins
Centro de Desenvolvimento da Tecnologia Nuclear, 31270-901 Belo Horizonte, MG, Brazil

 (Received 5 September 2018; revised manuscript received 19 December 2018; published 11 January 2019)

We investigate the ferromagnetic resonance modes of the magnetic vortex states on $\text{Ni}_{81}\text{Fe}_{19}$ ellipses using broadband ferromagnetic resonance measurements and micromagnetic simulations. Experiments show a rich structure of modes in the resonance absorption spectra, with absorption peak amplitudes dependent on the direction of the probing radio-frequency field. The evolution of the resonant modes is observed to be symmetric around zero field, due to the reversibility of the vortex core motion. The simulated absorption spectra reproduce the main features of the experimental results. A detailed analysis of the resonant modes at zero field shows that the observed absorption profiles result from the overlap of resonant modes which have an increasing complexity with the frequency. Besides, the simplest resonant modes are not those that exhibit the larger absorption amplitudes. Furthermore, the observed frequency splitting of some of the oscillation modes with the external field is correlated to the symmetry breaking during the vortex motion.

DOI: [10.1103/PhysRevB.99.014413](https://doi.org/10.1103/PhysRevB.99.014413)

I. INTRODUCTION

The understanding and control of the magnetization dynamics in patterned magnetic structures are important issues for both fundamental science and the design of new magnetic devices, particularly nanoscale devices for operations at microwave frequencies. A major role on the magnetization dynamics at these frequencies is played by the spin wave excitation for each individual magnetic element. A relevant case is the class of magnetic elements exhibiting vortex states, as is the case for disks and ellipses of low anisotropy materials. The magnetization dynamics of nano- and micron-sized circular and elliptical magnetic elements have been studied for saturated magnetization states [1–6]. Under the appropriate conditions, these elements also exhibit a magnetic vortex ground state consisting of an in-plane flux closure magnetic distribution and a small central core that is magnetized perpendicular to the plane. The spin wave excitation spectra in vortex-state magnetization include a low-frequency gyrotropic mode and high-frequency spin wave modes. Gyrotropic modes have been studied in disks [7–9] and ellipses [10–13]. High-frequency modes show radial and azimuthal symmetry in disks and have been extensively studied [1,3,6,8,9,14–20]. The spin wave dynamics in the case of elliptical NiFe dots was investigated with Brillouin scattering for saturated states [2,4] and *S*-like states [4], but not for single vortex states.

In this paper, we study the resonance modes of $\text{Ni}_{81}\text{Fe}_{19}$ ellipses in the magnetic field along the magnetization curve, including the vortex state, using broadband ferromagnetic resonance experiments and micromagnetic simulations. In Sec. II, we describe the experimental details and present the results. In Sec. III, we present the micromagnetic simulation approach, results, and comparison with the experiment. In Sec. IV, we present the conclusions of this paper.

II. EXPERIMENTAL METHODS AND MEASUREMENTS

A periodic array of ellipses was fabricated using *e*-beam lithography, sputtering, and lift-off processes. The array was patterned, over an area of $2 \times 2 \text{ mm}^2$, on a spin-coated layer of resist on a Si(100) substrate using a Raith *e*_LINE *e*-beam lithography system. A 50-nm-thick $\text{Ni}_{81}\text{Fe}_{19}$ layer was deposited over the patterned substrate by magnetron sputtering using a rf power source. The deposition conditions were 5 mTorr pressure and 50 sccm Ar gas flow, after a 5×10^{-8} Torr base pressure has been attained in the whole chamber. After lift-off, $2.4 \mu\text{m} \times 1.4 \mu\text{m}$ elliptical elements with smooth surfaces and no defects at the edges were obtained (see Fig. 1). The spacing between the edges of the elliptical elements are, respectively, 730 and 640 nm along the major and minor axis directions.

Measurements on remanence after saturating the ellipses along their minor axis direction (800 Oe in-plane magnetic field) result in most of the elements exhibiting a single vortex magnetic state. The magnetic domain image of this state, obtained by magnetic force microscopy (MFM), can be observed in the inset of Fig. 1. Very few ellipses with double vortex configurations were also observed, but statistically the formation of single vortex domains is expected if the ellipses were previously saturated on the minor axis [21].

The signature of single vortex states is also present in static magnetic measurements (M vs H) obtained with an alternating gradient field magnetometer (AGFM) [see Fig. 2(a)]. Starting from the negative saturated state, for the magnetic field H applied along the minor axis direction, the vortices start to nucleate at about -240 Oe. A well-defined linear and reversible response region is observed between ± 140 Oe. The reversible magnetization field range corresponds to a well-defined magnetic vortex state with a vortex core displacement proportional to H . Finally, at $+375$ Oe

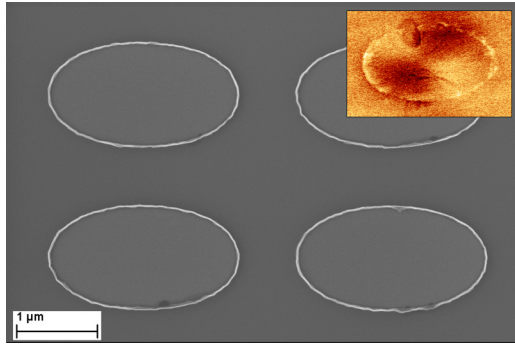


FIG. 1. Main figure: Scanning electron microscope image of the $2.4 \mu\text{m} \times 1.4 \mu\text{m}$ elliptical elements. Inset: Magnetic force microscopy image, showing the vortex configuration.

all vortices are annihilated and a positive saturation state is attained.

We have used a broadband ferromagnetic resonance setup for the dynamic measurements, as described in Ref. [22]. In this work, a dc magnetic field H sweeping from -550 to $+550$ Oe was always applied along the ellipses' minor axis direction. On the other hand, the radio-frequency probing fields h_{rf} were applied along the minor axis direction ($H \parallel h_{\text{rf}}$) or along the major axis direction ($H \perp h_{\text{rf}}$). The resulting absorbed power spectra are shown in Figs. 2(b) and 2(c) for

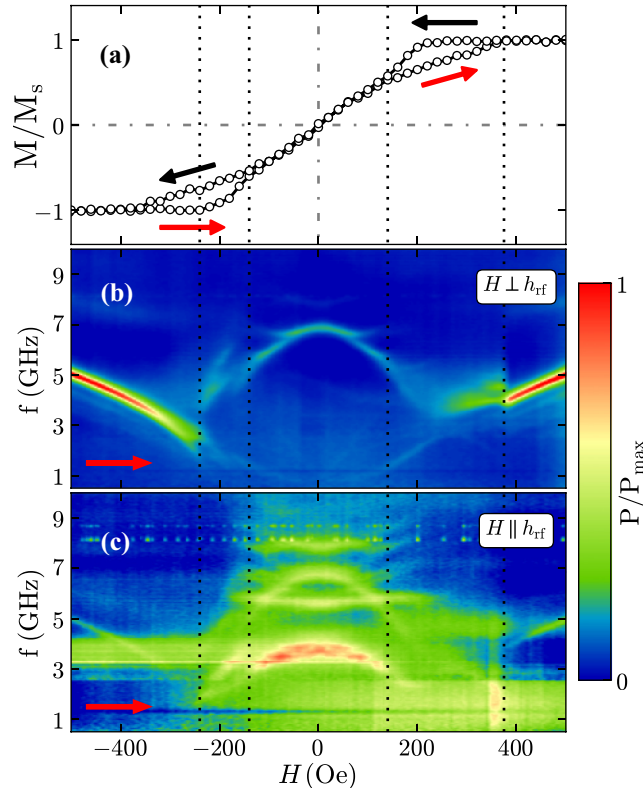


FIG. 2. (a) Magnetization curve. (b) and (c) Experimental absorbed power spectra for $H \perp h_{\text{rf}}$ and $H \parallel h_{\text{rf}}$, respectively. The vertical dotted lines correspond to the transition fields described in the text and the arrows indicate the field sweep direction.

frequencies ranging from 0.5 to 10.0 GHz. In these figures the color scale denotes the absorbed power amplitude. The largest absorption amplitudes are observed at the branches corresponding to the uniform resonance modes in the $H \perp h_{\text{rf}}$ spectra [Fig. 2(b)]. These branches, whose resonant frequencies f_r increase with H , appear only when the sample is saturated. The slope of the dispersion relation (f_r vs H) of these modes is dependent on the effective shape anisotropy of the array of ellipses as a whole. The other low-intensity branches observed in the saturation region in Fig. 2(b) are nonuniform modes [2,4].

For the purpose of contrast resolution, Fig. 2(c) uses the same color scheme as Fig. 2(b), but the experimental signal for $H \parallel h_{\text{rf}}$ is far smaller than for $H \perp h_{\text{rf}}$. This leads to an apparent larger noise and the observation of systematic error signals in Fig. 2(c). No absorbed power is theoretically expected for $H \parallel h_{\text{rf}}$ when the sample is saturated since the magnetization is not perturbed by h_{rf} pointing in the same direction. However, in Fig. 2(c), low-intensity branches at frequencies and fields corresponding to the uniform resonance mode are observed. This measured absorption is mostly due a small out-of-plane h_{rf} present in the experiment because the sample dimensions are larger than the central conductor width of the coplanar waveguide used.

At $H = 0$ Oe several absorption peaks corresponding to the vortex-state resonances are observed. For $H \perp h_{\text{rf}}$ the more intense peak is around 6.8 GHz and other low-intensity peaks are observed for lower and higher frequencies. The resonant branch of the 6.8-GHz peak evolves with H to lower resonance frequencies, and then splits into two branches at around 65 Oe. These features are not compatible with a single resonant mode, indicating a possible superposition of two or more modes with different dispersion relations. On the other hand, for $H \parallel h_{\text{rf}}$, the larger absorption at $H = 0$ Oe is not observed as a single peak, but for a broad frequency range (from 3.2 to 4.5 GHz), indicating a clear superposition of several resonance modes. The same absorption profile and field evolution of the 6.8-GHz peak observed for $H \perp h_{\text{rf}}$ can also be perceived from Fig. 2(c). Other resonant branches are also present.

When H along the minor axis orientation is applied, the vortex cores move along the major axis, with the direction dependent on the vortex chirality and H sign. Experimentally, a symmetry on the absorption spectra is observed around $H = 0$ (see Fig. 2): The same resonant modes are observed as long as the amplitude of H lies in the reversible part of the magnetization curve. The same behavior was reported for a vortex in a disk [23].

Considering that we do not control the chirality on our ellipse, both possible vortex core motions result in the same absorption response. The abrupt frequency changes in the resonant branches at $H = -140$ Oe indicate an intermediate magnetic state between saturation and the displaced vortex state. A similar behavior is observed for $H > 250$ Oe where clearly different resonant modes are observed.

From the differences in the absorption spectra for $H \parallel h_{\text{rf}}$ and $H \perp h_{\text{rf}}$ it is clear that the direction of h_{rf} largely influences which resonant modes are excited and, subsequently, absorb microwave power. In order to investigate the resonant modes in further detail, we have analyzed the broadband

ferromagnetic response of a single ellipse with the support of micromagnetic simulations.

III. MICROMAGNETIC SIMULATIONS AND ANALYSIS

We have used the MUMAX3 [24] software to perform micromagnetic simulations of a magnetic ellipse, discretized with a cell size $7.14 \times 7.14 \times 50 \text{ nm}^3$ using a simulation box of $336 \times 196 \times 1$ cells. This corresponds to the shape and size of a single ellipse of our experimental sample. The parameters used for the magnetic material were as follows: saturation magnetization $M_s = 800 \times 10^3 \text{ A/m}$, exchange constant $A = 1.3 \times 10^{-11} \text{ J/m}$, and damping constant $\alpha = 0.02$. The simulations were carried on a field frequency (H, f) , with H ranging from 0 to 260 Oe, field steps of 5 Oe, f ranging from 0.5 to 10.0 GHz, and frequency steps of 100 MHz.

The static magnetic vortex configurations along the H range are calculated by gradually increasing H and relaxing from the previously calculated magnetic configuration. For $H = 0 \text{ Oe}$, the initial magnetization is set as a numerically generated vortex which after relaxation leads to a vortex configuration inside the ellipse, resulting in a vortex core of around 70-nm diameter (10×10 simulation cells).

The simulation routines for the dynamical response aim to reproduce the procedure of the broadband ferromagnetic resonance experiment. For each H , a fixed frequency h_{rf} is applied and the response is recorded after a stable harmonic oscillation is attained. This procedure is repeated for all the frequencies to be measured. Finally, software developed by our research group is used to process the recorded data in order to obtain the absorbed power spectra comparable with the experimental data and the oscillation modes.

For every point in the (H, f) grid the absorbed power amplitudes are calculated from the area inside the minor hysteresis loop created by h_{rf} and the oscillating part of the magnetization along the h_{rf} direction. For the oscillation modes we calculate the amplitude and phase of the first harmonic response for each cell in our simulation box. For easier analysis of the modes, instead of using the usual xyz coordinates defined by the frame of the simulation box, we express the oscillating part of the magnetization in the components perpendicular to the local static magnetization vectors. Furthermore, as the vortex core is small and the out-of-plane components are also small in amplitude due to the shape anisotropy, we will present only the in-plane oscillation components.

No appreciable dynamical change of the vortex core position is observed for any of the analyzed frequencies. Instead, the observed spin oscillations occur in the volume of the ellipse.

In Fig. 3 we show the simulated absorbed power spectra and the experimental results for H in the 0–300 Oe range. The color scale used maximizes the contrast in the presented H and f range. As seen from the figure, the main features of the experimental results are reproduced in the simulated spectra. The shapes and relative amplitudes of the absorption branches are well reproduced. However, the simulated absorption peaks occur at higher frequencies than their experimental counterparts. We attribute these frequency discrepancies to magnetic anisotropies not taken into account in our simula-

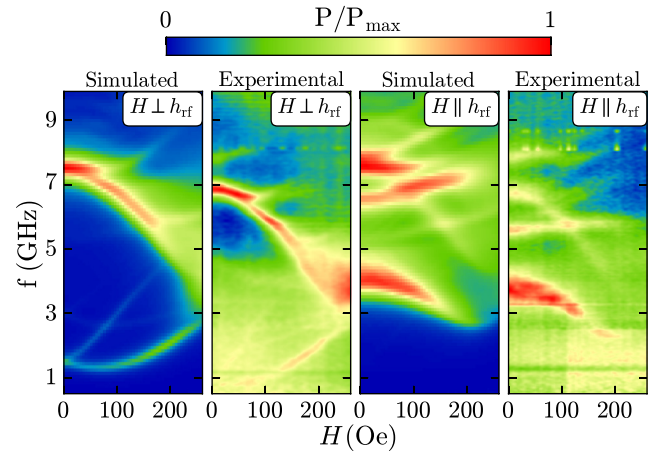


FIG. 3. Experimental and simulated absorbed power spectra for $H \perp h_{\text{rf}}$ and $H \parallel h_{\text{rf}}$.

tions. Particularly, a single ellipse element is simulated, while the experimental measurement is on an array of ellipses, thus, both systems have different effective shape anisotropies.

In order to get deeper insight on the dynamical behavior of our system, we analyze the simulated absorbed power profiles at $H = 0$, as shown in Fig. 4. We expect that each absorption peak corresponds to a natural oscillation mode with a characteristic resonant frequency f_r . The amplitude of the peaks depends on the h_{rf} efficiency to excite the corresponding oscillation modes and the linewidths are proportional to the effective magnetic damping. For $H \perp h_{\text{rf}}$ (black squares in Fig. 4), the most intense peak is observed at 7.5 GHz, which corresponds to the experimental peak observed at 6.8 GHz (see Fig. 3). The wide and asymmetric base of this peak indicates the presence of overlapping resonant peaks. Smaller but symmetric peaks are also observed at 1.5 and 3.0 GHz. On the other hand, for $H \parallel h_{\text{rf}}$ (red circles in Fig. 4), very broad and asymmetric peaks are observed, with maxima at 4.0, 6.6, and 7.6 GHz. This profile indicates the presence of several oscillation modes with very close resonant frequencies.

Besides the resonant frequencies, the oscillation modes are characterized by the spatial distribution of the oscillating magnetization M_{osc} . From our numerical simulations we obtain the amplitude and phase of M_{osc} . For all analyzed modes, the

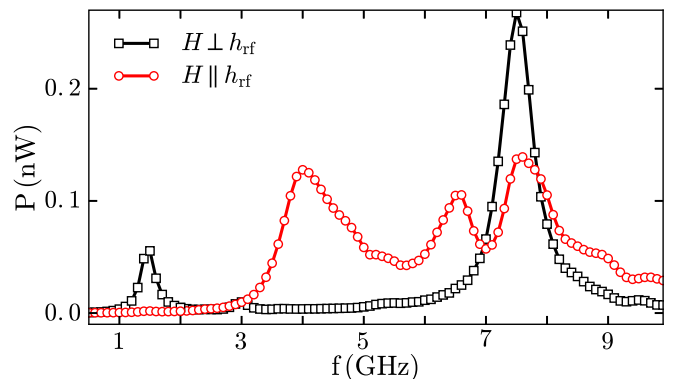


FIG. 4. Calculated absorbed power of one ellipse, as a function of frequency and h_{rf} direction, for $H = 0$ and $0.5 \text{ Oe } h_{\text{rf}}$ amplitude.

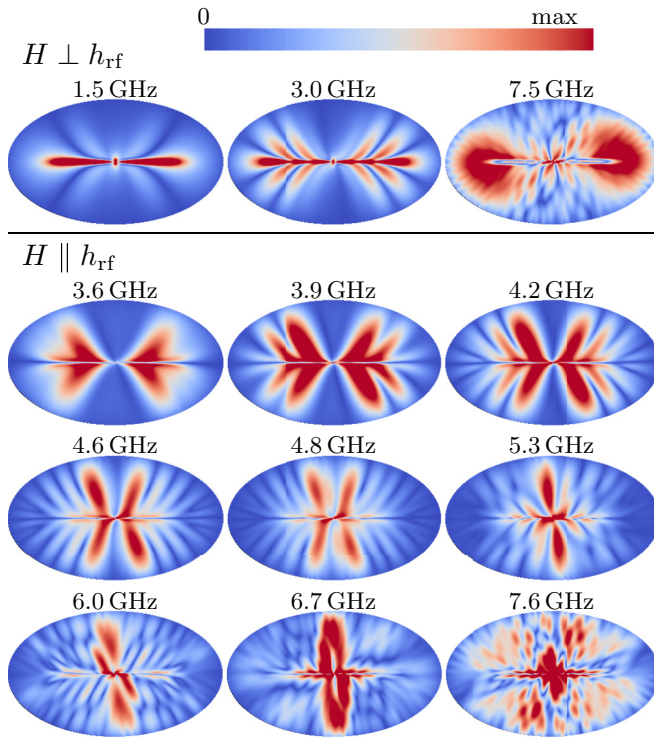


FIG. 5. Main modes' in-plane component of the magnetization oscillations at $H = 0$ Oe. Top: h_{rf} along the major axis. Bottom: h_{rf} and along the minor axis.

in-plane component of M_{osc} is mostly in quadrature ($\pm\pi/2$ phase difference) with h_{rf} at f_r , and there is no continuous variation of the phase with respect to the position. Therefore, we are in fact observing standing spin waves, in remarkable contrast to what is observed in disks, where spin waves circulate around the vortex core [3,8,14,16–18].

The in-plane M_{osc} amplitudes of the main modes, for $H = 0$, are shown in Fig. 5. For $H \perp h_{rf}$, the f_r of the plotted modes corresponds to the main peaks observed in Fig. 4. For $H \parallel h_{rf}$ we plotted selected oscillation modes with f_r all along the absorbed power profile. For frequencies below 4.8 GHz, we observe standing spin waves with the wave vector locally parallel to the static magnetization. The wavelength decreases with increasing frequency, and consequently the observed number of nodes gradually increase. The simplest mode observed corresponds to the absorption peak at 1.5 GHz, where only two large intensity antinodes are observed. For frequencies higher than 4.8 GHz we observe mixed oscillation modes, with wave vectors parallel and perpendicular to the static magnetization.

The mode observed at 1.5 GHz deserves special attention: The spatial amplitude distribution for this mode follows the same pattern of the magnetic free-energy spatial distribution (not shown). The regions along the major axis have a larger magnetization curling when compared to the curling along the minor axis. This indicates an increased exchange energy along the major axis which corresponds to the zones with a larger amplitude for this particular mode. This increased local exchange energy also acts as a pinning point for the spin waves. The magnetization curling changes and associated exchange

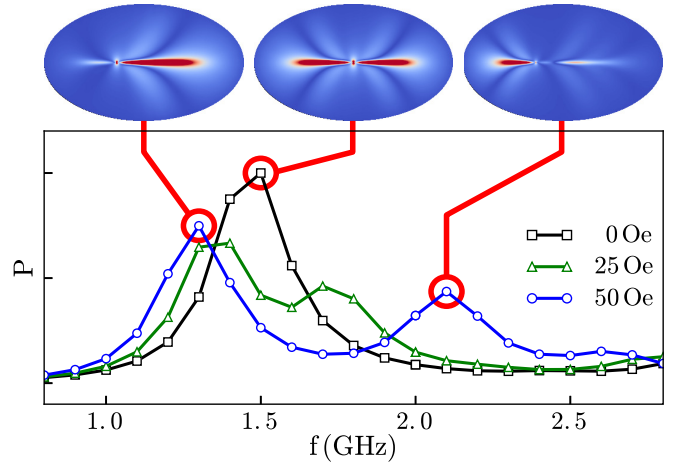


FIG. 6. Vortex core motion and frequency splitting of the 1.5-GHz mode due to an applied external field.

energy both depend on the ellipse aspect ratio. Numerical simulations show that aspect ratios larger than 1.3 exhibit the behavior just explained. Furthermore, for ellipses with different sizes, preliminary simulations indicate that the mode at 1.5 GHz is intrinsically related to the exchange energy as the frequency and amplitude increase for smaller ellipses. In the case of the mode observed at 7.5 GHz, the dipolar energy seems to be dominant as both the oscillation amplitude and frequency are almost unchanged for different ellipse sizes.

As stated in the previous section, the field evolution of the absorbed spectra shows an overlap of resonant peaks. This makes it difficult to identify the individual oscillation modes and analyze their field dependence. A particular case is the 1.5-GHz absorption peak observed for $H = 0$ in the $H \perp h_{rf}$ simulated spectra, where a single peak is observed. When H is increased, the single peak splits into two different resonant branches, one with continuously increasing f_r and decreasing absorption amplitude. The second resonant branch first decreases in f_r for H up to 60 Oe and then also increases f_r with H . Furthermore, this branch continuously increases its absorption amplitude with H . The experimental counterpart of these features can also be observed in Fig. 3. Additionally, the 3.0-GHz peak observed for $H = 0$ in the $H \perp h_{rf}$ simulated spectra also behaves in this way, although with a far lower absorption amplitude.

The frequency splitting due to the in-plane field has been observed already for resonance modes in permalloy disks [3]. In this paper, numerical simulations allow us to have a better understanding of this behavior. As it can be seen from Fig. 6, for $H = 0$, a single absorption peak with $f_r = 1.5$ GHz is observed. The corresponding oscillation mode is symmetric with respect to the vortex core and shows two antinodes with equal amplitudes, along the major ellipse axis. When a field is applied, the vortex core is displaced, breaking the symmetry in the ellipse magnetic configuration. In this case, the two regions at each side of the vortex are different. The resonant frequency of the shrinking region (top right mode in Fig. 6) rapidly increases with H as the contributions to exchange, dipolar, and Zeeman energies increase. On the other hand, in the growing region (top left mode in Fig. 6), the exchange

and dipolar energies decrease with H . This leads to an initial frequency drop, but with larger H the frequency rises as the Zeeman energy becomes dominant. Furthermore, the amplitudes of the peaks depend on the oscillating volume of the modes, clearly explaining the observed amplitude differences in these modes.

IV. CONCLUSIONS

In this paper, we have produced arrays of micron-sized $\text{Ni}_{81}\text{Fe}_{19}$ ellipses. A static magnetic characterization (M vs H and MFM images) indicates single vortex structures for the magnetization in most of the ellipses.

The experimental studies of microwave absorption indicate that the microwave modes were found to be characteristic of each element of the array. Moreover, they are clearly associated with the vortex structure present in the ellipses. The microwave experiments were performed for microwave field directions perpendicular and parallel to the major axis, which in turn allows us to excite complementary vortex oscillation modes. The experimental results were well reproduced by

micromagnetic simulations that give access to the spatial distributions of magnetization oscillations, allowing us to identify the spin wave excitation modes. The modes follow the symmetry of the magnetic free energy and evolve with the applied dc field. In particular, for the vortex state, the order of the oscillation modes increases with the frequency. For lower frequencies, modes with a wave vector parallel to the magnetization were observed. As the frequency increases, modes with a wave vector perpendicular to the magnetization are also observed.

These results will help understand and provide insight into the magnetization dynamics in vortex systems in confined elliptical conditions, opening further perspectives for the tailoring of magnonic devices.

ACKNOWLEDGMENTS

This work was supported by the Brazilian agencies CNPq, CAPES, FAPEMIG, and FAPERJ. We also acknowledge the LABNANO/CBPF and LABSURF/CBPF for the nanofabrication infrastructure.

-
- [1] L. Giovannini, F. Montoncello, F. Nizzoli, G. Gubbiotti, G. Carlotti, T. Okuno, T. Shinjo, and M. Grimsditch, *Phys. Rev. B* **70**, 172404 (2004).
- [2] G. Gubbiotti, G. Carlotti, T. Okuno, M. Grimsditch, L. Giovannini, F. Montoncello, and F. Nizzoli, *Phys. Rev. B* **72**, 184419 (2005).
- [3] I. Neudecker, K. Perzlmaier, F. Hoffmann, G. Woltersdorf, M. Buess, D. Weiss, and C. H. Back, *Phys. Rev. B* **73**, 134426 (2006).
- [4] F. Montoncello, L. Giovannini, F. Nizzoli, P. Vavassori, M. Grimsditch, T. Ono, G. Gubbiotti, S. Tacchi, and G. Carlotti, *Phys. Rev. B* **76**, 024426 (2007).
- [5] V. V. Naletov, G. de Loubens, G. Albuquerque, S. Borlenghi, V. Cros, G. Faini, J. Grollier, H. Hurdequint, N. Locatelli, B. Pigeau, A. N. Slavin, V. S. Tiberkevich, C. Ulysse, T. Valet, and O. Klein, *Phys. Rev. B* **84**, 224423 (2011).
- [6] V. Castel, J. Ben Youssef, F. Boust, R. Weil, B. Pigeau, G. de Loubens, V. V. Naletov, O. Klein, and N. Vukadinovic, *Phys. Rev. B* **85**, 184419 (2012).
- [7] J. P. Park, P. Eames, D. M. Engebretson, J. Berezovsky, and P. A. Crowell, *Phys. Rev. B* **67**, 020403 (2003).
- [8] C. E. Zaspel, B. A. Ivanov, J. P. Park, and P. A. Crowell, *Phys. Rev. B* **72**, 024427 (2005).
- [9] K. Y. Guslienko, X. F. Han, D. J. Keavney, R. Divan, and S. D. Bader, *Phys. Rev. Lett.* **96**, 067205 (2006).
- [10] K. S. Buchanan, P. E. Roy, M. Grimsditch, F. Y. Fradin, K. Y. Guslienko, S. D. Bader, and V. Novosad, *Phys. Rev. B* **74**, 064404 (2006).
- [11] K.-S. Lee, Y.-S. Yu, Y.-S. Choi, D.-E. Jeong, and S.-K. Kim, *Appl. Phys. Lett.* **92**, 192513 (2008).
- [12] G. Lv, H. Zhang, X. Cao, F. Gao, and Y. Liu, *Appl. Phys. Lett.* **103**, 252404 (2013).
- [13] C. Zaspel, *J. Magn. Magn. Mater.* **433**, 59 (2017).
- [14] M. Buess, R. Höllinger, T. Haug, K. Perzlmaier, U. Krey, D. Pescia, M. R. Scheinfein, D. Weiss, and C. H. Back, *Phys. Rev. Lett.* **93**, 077207 (2004).
- [15] M. Buess, T. P. J. Knowles, R. Höllinger, T. Haug, U. Krey, D. Weiss, D. Pescia, M. R. Scheinfein, and C. H. Back, *Phys. Rev. B* **71**, 104415 (2005).
- [16] X. Zhu, Z. Liu, V. Metlushko, P. Grütter, and M. R. Freeman, *Phys. Rev. B* **71**, 180408 (2005).
- [17] J. P. Park and P. A. Crowell, *Phys. Rev. Lett.* **95**, 167201 (2005).
- [18] F. G. Aliev, J. F. Sierra, A. A. Awad, G. N. Kakazei, D.-S. Han, S.-K. Kim, V. Metlushko, B. Ilic, and K. Y. Guslienko, *Phys. Rev. B* **79**, 174433 (2009).
- [19] A. A. Awad, K. Y. Guslienko, J. F. Sierra, G. N. Kakazei, V. Metlushko, and F. G. Aliev, *Appl. Phys. Lett.* **96**, 012503 (2010).
- [20] R. V. Verba, A. Hierro-Rodriguez, D. Navas, J. Ding, X. M. Liu, A. O. Adeyeye, K. Y. Guslienko, and G. N. Kakazei, *Phys. Rev. B* **93**, 214437 (2016).
- [21] P. Vavassori, N. Zaluzec, V. Metlushko, V. Novosad, B. Ilic, and M. Grimsditch, *Phys. Rev. B* **69**, 214404 (2004).
- [22] D. E. Gonzalez-Chavez, R. Dutra, W. O. Rosa, T. L. Marcondes, A. Mello, and R. L. Sommer, *Phys. Rev. B* **88**, 104431 (2013).
- [23] F. G. Aliev, A. A. Awad, D. Dieleman, A. Lara, V. Metlushko, and K. Y. Guslienko, *Phys. Rev. B* **84**, 144406 (2011).
- [24] A. Vansteenkiste and B. V. de Wiele, *J. Magn. Magn. Mater.* **323**, 2585 (2011); see <http://mumax.github.io/3>.